



A global database of extreme fire events from satellite data from 2003 to 2022

Erika Solano-Romero¹, Carlota Segura-Garcia¹, M. Lucrecia Pettinari¹, Amin Khairoun¹, Miguel Ángel Torres-Vázquez¹, Emilio Chuvieco¹

¹ Environmental Remote Sensing Research Group, Department of Geology, Geography and the Environment, Universidad de Alcalá, Calle Colegios 2- Alcalá de Henares, 28801, Spain

Correspondence to: Erika Solano-Romero (erika.solano@uah.es)

Abstract. Extreme fires represent a significant threat due to their impacts on climate, ecosystems, and society. Despite their increasing prevalence, their definition remains controversial, as their characteristics vary depending on the region considered. In this article, we present the first version of the Extreme Fire Events (EFEs) database, a global dataset of extreme fires in NetCDF format containing monthly rasters on a regular grid with a spatial resolution of 0.25 degrees. The database includes the period 2003-2022, when a consistent satellite record was available. The basic unit of analysis is a cell-month event (CME), which represents aggregated fire activity within a grid cell during a given month. The identification of extreme events was based on two main satellite-derived variables: Burned Area (BA) from the European Space Agency's FireCCI51 dataset and Fire Radiative Power (FRP) obtained from the NASA MCD14ML active fire product. Both variables were derived from the MODIS sensor. They were aggregated to the spatial and temporal scale defined for the CMEs and were used to compute standardised anomalies within each of the 55 defined regions, in order to account for spatial and seasonal differences in fire activity in the main global biomes. A CME was classified as an EFE when it presented anomalous values in both variables according to the established regional thresholds. Further, for each EFE, the database also indicates if any fire perimeter from the FRY v2.0 dataset identified as extreme by a certain attribute (fire size, duration, mean FRP, rate of spread and severity) overlapped with the CME. The database includes 19,951 EFEs between 2003 and 2022, with the highest frequency in 2010 and 2007, and the lowest in 2013. The dataset is intended for climate and Earth System modellers aiming to understand the causes and impacts of EFEs, as well as to forecast their occurrence under future scenarios or include them in broader Earth System models.

1 Introduction

Wildfires have significant impacts on the climate, ecosystems, and society, including effects on vegetation, soil, water resources, and human health (Bell et al., 2018; Bowman et al., 2020a). Recent global trends show a decrease in total burned area (BA), mainly attributed to land-use changes and human management in savannas and grasslands (Andela et al., 2017). Paradoxically, recent studies also indicate that extreme wildfires (here understood as unusually large or intense events) are



34 becoming more frequent across many regions of the world (Cunningham et al., 2024; Abatzoglou et al., 2025; Cunningham et
35 al., 2025a). Indeed, extraordinary fire seasons have been observed across different regions of the world over the past few years.
36 For example, in 2017, the wildfire in Pedrógão Grande, Portugal, devastated over 9,000 hectares and caused 66 fatalities,
37 becoming the deadliest wildfire in the country's history and one of the most tragic in Europe (Pinto et al., 2022). Shortly
38 thereafter, the 2019-2020 "Black Summer" fire season in Australia was unprecedented in both scale and intensity (Abram et
39 al., 2021), with many areas in the South East of the country burning around eight times more than in the previous 18 years
40 (Bowman et al., 2020b). Following this trend, in 2021, almost 8.5 million hectares of forests burned in Yakutia, Siberia,
41 marking one of the largest wildfires in Russia and globally for that year (Desyatkin et al., 2024). Together, these events
42 illustrate some of the impacts of extreme wildfires within the period covered by our study.

43 The occurrence of these extreme fire events (EFEs) and their disproportionate impacts on humans, ecosystems and the climate,
44 have led to an increasing number of scientific publications (Bowman et al., 2017; Tedim et al., 2018; Linley et al., 2022;
45 Cunningham et al., 2024). However, there is still no unique approach to defining or characterising extreme events. Indeed,
46 different criteria have been proposed to characterise these events, considering parameters such as fire size (Tedim et al., 2018;
47 Linley et al., 2022), intensity (Cunningham et al., 2024), or even the capacity to suppress the fire (Bowman et al., 2017; Tedim
48 et al., 2018; Linley et al., 2022). For example, to simplify the characterization, some authors proposed the use of thresholds of
49 fire size (e.g., > 10,000 ha) to consider an individual fire event, or a cluster of fires, as extreme (Linley et al., 2022, 2025;
50 Ghasemiazma et al., 2026). However, even if the mechanisms underlying fire behaviour might be universal, the typical patterns
51 of fire differ considerably between regions of the world due to specific ecological and climatic conditions (Archibald et al.,
52 2013; García et al., 2022; Yin et al., 2026). Consequently, the use of unique global thresholds may not be suitable to
53 characterize EFEs essentially because large or intense fires that may be relatively common in some regions may have disastrous
54 impacts in others (Tedim et al., 2018; Jones et al., 2024). In addition, fires in fuel-limited regions (e.g., deserts or agricultural
55 areas) may never reach large extents (e.g., fire sizes above 10,000 ha), even under a strong climatic influence on interannual
56 fire variability, which limits the applicability of global fire behaviour thresholds (Bowman et al., 2017; Gincheva et al., 2024).
57 Many of the most EFEs that occurred in the last few years have taken place in regions with high fuel availability, leading to
58 long-lasting large-scale disturbances that can alter vegetation structure, species composition and ecosystem dynamics over
59 long periods (Duane et al., 2021). Consequently, EFEs can contribute to amplifying climate change by releasing large amounts
60 of greenhouse gases and particles (Peterson et al., 2021; Kelley et al., 2025) and causing large impacts on water (Adams, 2013)
61 and air quality (Kelley et al., 2025). Therefore, even though extreme fires occur sporadically, these events can play a
62 disproportionate role in shaping landscapes (Meyn et al., 2007; Jones et al., 2022).

63 In recent years, several global products on fire activity derived from satellite observations have been released (Chuvieco et al.,
64 2020), thus facilitating the analysis of fire impacts and drivers (Jones et al., 2024; Kelley et al., 2025). However, the analysis
65 of EFEs remains limited, due to both the lack of a standard definition of their characteristics and the absence of a dedicated
66 database that would facilitate the analysis of different fire event typologies and drivers. This was the main objective of the
67 XFIRES project (European Space Agency, 2026), funded under the cross-ECV (Essential Climate Variables) activities of the

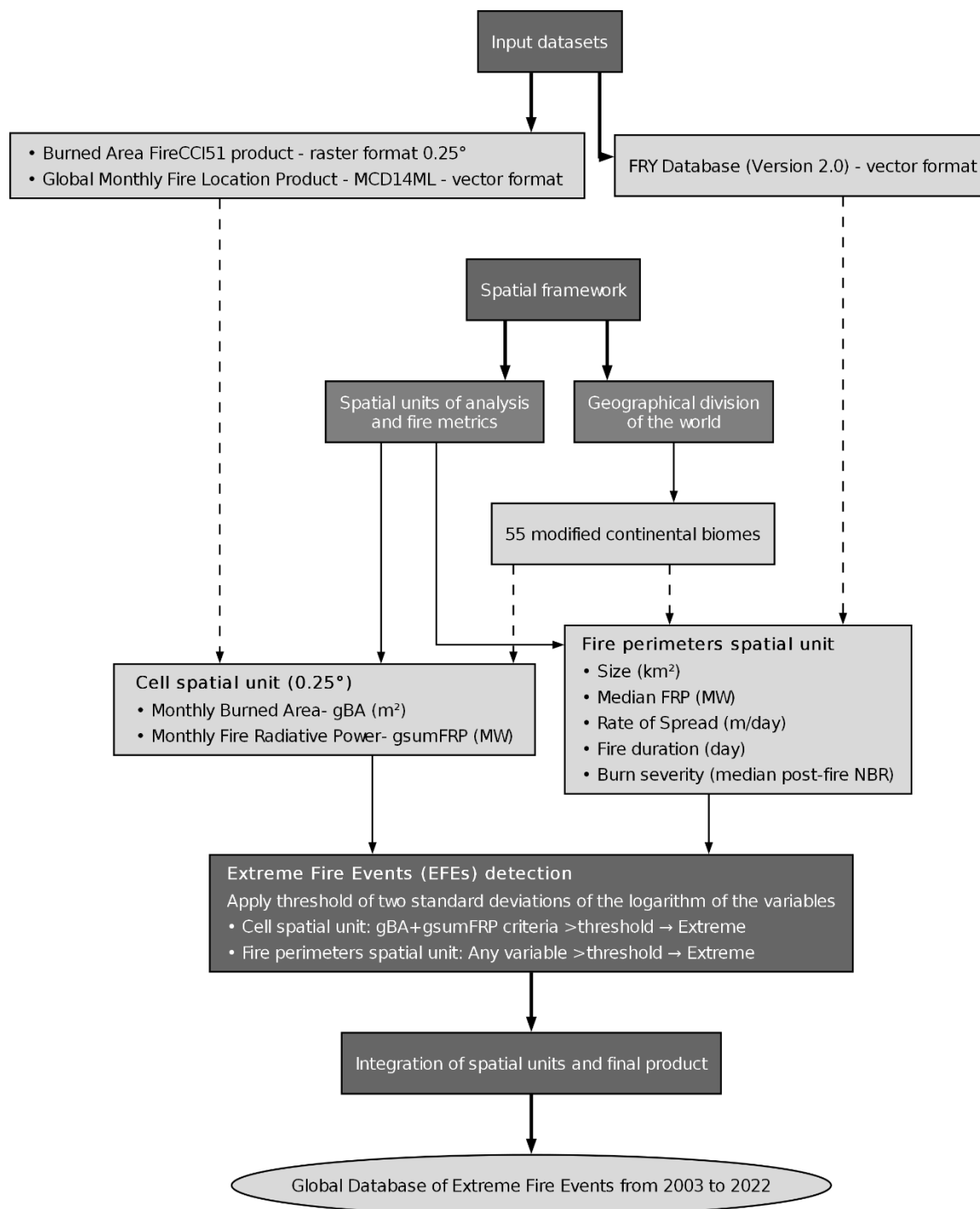


68 European Space Agency (ESA). The aim of this paper is to present the first version of this global EFEs database. The database
69 covers the period 2003-2022 and is based on satellite-derived BA and Fire Radiative Power (FRP), aggregated to a monthly
70 0.25-degree grid, where the fire activity of each grid cell in each month constitutes a fire event (hereafter called cell-month
71 events, CMEs). The period was selected to ensure the use of consistent long-term datasets and to include years with different
72 global fire characteristics. CMEs were identified as extreme using regionally standardized anomalies of BA and FRP, and the
73 resulting EFEs database includes information on monthly values of both variables, as well as auxiliary data derived from the
74 analysis of fire perimeters, indicating which characteristics such as size, duration, mean FRP, rate of spread, or severity of the
75 fire event stand out as extreme. This allows the database to retain CMEs as the main analytical unit while providing
76 supplementary information on fire event characteristics within the associated fire perimeters. This provides a consistent
77 framework for assessing extreme fire activity, both spatially and temporally.

78 **2 Methods**

79 Figure 1 presents the workflow used to construct the EFEs database for the period 2003-2022. The dataset is based on BA and
80 FRP derived from satellite observations, aggregated monthly on a 0.25° grid, capturing complementary aspects of fire activity:
81 BA reflects the spatial extent of fires over a CME, while the sum of FRP represents an estimate of the rate of radiative energy
82 release and fire intensity. To account for regional variability, the world was divided into 55 regions corresponding roughly to
83 continental biomes. Thresholds of BA and sum of FRP were then calculated independently for each region and fire variable
84 using standardised anomalies. Finally, a CME was considered to be an EFE when both its BA and the sum of FRP values
85 exceeded their corresponding regional thresholds. In addition to CMEs, fire perimeters were assessed for extreme
86 characteristics using the same standardised anomaly approach. For each EFE (i.e., an extreme CME), overlapping fire patches
87 were examined to determine whether they were extreme for any given attribute. The database records this information as a
88 binary indicator of extremeness for size, duration, mean FRP, rate of spread, or burn severity, rather than providing the
89 quantitative values. Fire perimeters information was extracted from the FRY v2.0 dataset (Laurent et al., 2018; Chen, 2025).

90



91

92

Figure 1: Workflow for constructing the database of global Extreme Fire Events (EFEs) in the period 2003 to 2022.

93



94 **2.1 Input datasets**

95 To construct the EFEs database, we used data from three main datasets providing information on fire activity at a global scale.

96 **2.1.1 FireCCI51 global burned area dataset**

97 FireCCI51 (Lizundia-Loiola et al., 2020) is a global BA dataset developed under the ESA FireCCI project (European Space
98 Agency, 2025a) provided in pixel (~250 m and daily) and grid (0.25° and monthly) format. Both pixel and grid datasets provide
99 consistent global BA records for the period 2001-2022 using advanced detection algorithms and improved uncertainty
100 characterisation (European Space Agency, 2025a) and are publicly available through the Centre for Environmental Data
101 Analysis (CEDA) Archive catalogue (Chuvieco et al., 2019). FireCCI51 pixel product algorithm combines spectral information
102 from the MODIS sensor, integrating near-infrared (NIR) reflectance bands (~250 m) with the detection of active fires (AFs)
103 from mid-infrared and thermal channels. This approach is developed in two phases: first, it identifies pixels affected by fires
104 through thermal anomalies, and then it expands the detection by considering the reduction in near-infrared reflectance between
105 images taken before and after the event, allowing for a more precise delimitation of the BAs (Lizundia-Loiola et al., 2020). In
106 this study, we used the FireCCI51 grid product, which is provided as monthly NetCDF files, representing monthly and spatially
107 aggregated BAs of the FireCCI51 pixel product to a regular grid with a spatial resolution of 0.25°. We used BA for the period
108 2003-2022, corresponding to the years of stable operation of the Terra (launched in December 1999) and Aqua (launched in
109 May 2002) satellites to ensure the continuity and temporal reliability of the series of burned areas analysed (Lizundia-Loiola
110 et al., 2020).

111 **2.1.2 Global Monthly Fire Location and FRP Product - MCD14ML**

112 The MCD14ML is a satellite product based on data from MODIS sensors aboard NASA's Terra and Aqua satellites (Collection
113 6.1) providing detections of AFs globally (Giglio et al., 2021). The daily MOD14 (Terra) and MYD14 (Aqua) products provide
114 these individual detections with a spatial resolution of approximately 1 km per pixel at nadir (Giglio et al., 2016). The MODIS
115 AFs detection algorithm identifies thermal anomalies on the Earth's surface and determines which ones correspond to fires.
116 Each MCD14ML record corresponds to an AF pixel and includes coordinates, acquisition time, thermal source type, and
117 confidence level. The thermal source type is numerically coded: suspected vegetation fire (0), active volcano (1), other static
118 terrestrial source (2), and maritime source (3) (Giglio et al., 2021). Further, MCD14ML also includes an estimate of the FRP
119 of the AF, estimated in megawatts (MW), which quantifies the instantaneous thermal energy emitted by a fire at the satellite
120 overpass, and is commonly used to estimate the intensity of the fire (Giglio et al., 2021).

121 **2.1.3 FRY Database (Version 2.0)**

122 As a complementary information to the CMEs, we incorporated into the EFE database burned perimeters information derived
123 from the FRY v2.0 dataset (Laurent et al., 2018; Chen, 2025). This product provides detailed information on different



124 characteristics of individual fire patches in vector format (Laurent et al., 2018). Each fire perimeter is identified by applying a
125 ‘flood-fill’ clustering algorithm (Archibald and Roy, 2009) to draw fire polygons and characterise their features (Laurent et
126 al., 2018). The algorithm considers contiguous burned pixels to be part of the same perimeter if they coincide within a temporal
127 period below a set “cut-off” value (Laurent et al., 2018). FRY provides fire perimeters using two temporal cut-off values, 6
128 and 12 days (Chen, 2025). In regions such as the tropical and subtropical savannas of Africa, very large fire perimeters can
129 result from the thresholds applied by the FRY algorithm, as multiple adjacent fires occurring within a short period may be
130 aggregated into a single patch (Figure S1). In this study, we used fire perimeters derived from the FireCCI51 product with the
131 12-day cut-off, to account for the uncertainty associated with the day of detection of the fires identified by FireCCI51
132 (Lizundia-Loiola et al., 2020). The FRY dataset is provided in the form of annual shapefiles of fire perimeters, which includes
133 a set of morphological attributes and fire behaviour variables describing individual fires. We considered fire size (in km²);
134 median fire FRP (in MW); median burn severity, derived from the MODIS Burn Severity dataset (MOSEV; Alonso-González
135 and Fernández-García (2021)); fire duration; and rate of spread (ROS), defined by the FRY dataset as fire size divided by
136 duration. These variables capture different dimensions of fire (spatial magnitude, energy intensity, temporal dynamics, and
137 ecological severity), which are and have been identified as key metrics for characterising fires on a global scale (Laurent et al.,
138 2018).

139 **2.2 Spatial units of analysis and fire metrics**

140 The construction of the EFEs database was based on two primary variables derived from satellite observations: BA and the
141 sum of FRP within a 0.25° grid cell and month (hereafter referred to as gBA and gsumFRP, respectively). These variables
142 were selected because they capture complementary dimensions of fire activity. BA is a primary metric for monitoring fire
143 extent and is extensively used in studies of large-scale fire activity (Mouillot et al., 2014), while the sum of FRP values from
144 AFs represents an estimation of the radiative energy released by the fire and has previously been used to characterise fire
145 intensity and extreme fire behaviour (Bowman et al., 2017; Cunningham et al., 2024).

146 As the EFEs database is targeted at climate and Earth System modellers, we identified extreme fire activity on a regular 0.25°
147 grid cell to facilitate its analysis with biophysical and socio-economic variables, which are also available in grid format. The
148 BA and FRP were aggregated in monthly periods. While the FireCCI51 BA product in grid format is directly provided with
149 these spatial and temporal resolutions, we aggregated the FRP values from the filtered AFs from MODIS into monthly FRP
150 sums. Therefore, we define CMEs as those grid cells with some fire activity in terms of BA or the sum of FRP in a certain
151 month. This approach allows a certain flexibility in characterising extreme fire activity, as extreme CMEs may correspond
152 either to a single extraordinary large and intense fire or to the anomalous accumulation of several individual fires that, together,
153 correspond to a large extent and energy emitted (Beverly and Schroeder, 2024). Aggregating fire activity at the monthly scale
154 offers a compromise between very short temporal resolutions (such as daily observations) which can artificially fragment
155 prolonged fire events and overestimate fire frequency, and the need to define broader temporal windows such as fire seasons,
156 whose duration varies considerably among regions (Archibald et al., 2013).



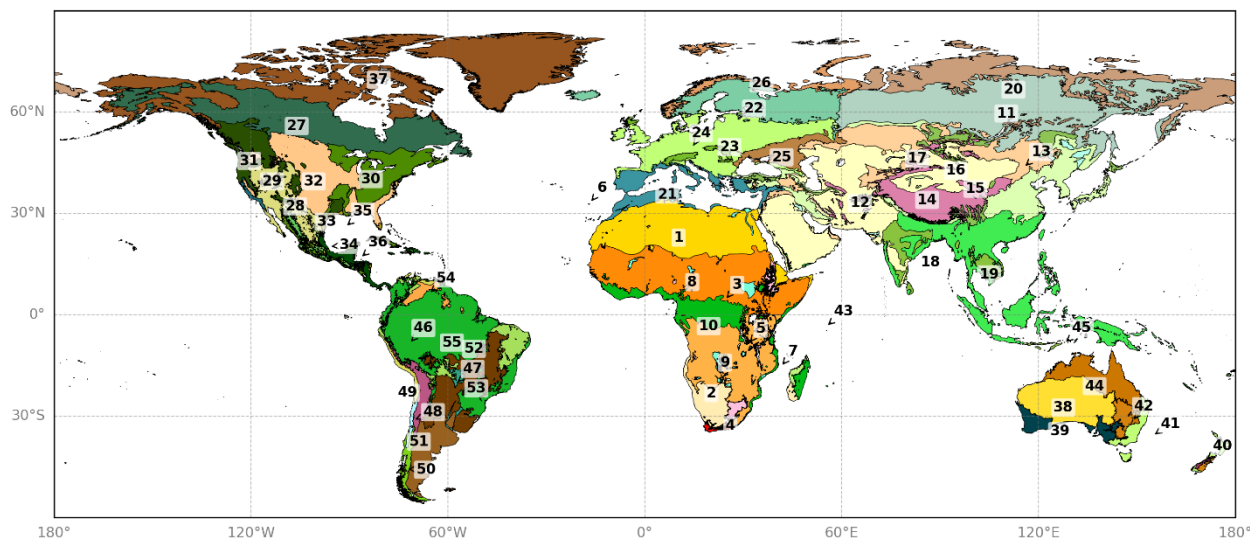
157 Moreover, grid-based approaches at comparable spatial scales to the one used here have been widely adopted in large-scale
158 fire studies, where fire activity is aggregated to grid cells over a certain period and considered as “fire events” (Bowman et al.,
159 2017; Cunningham et al., 2024). Monthly grid-based resolutions are also standard in global fire, climate, and vegetation
160 modelling frameworks, including Dynamic Global Vegetation Models (DGVMs) and Earth System Models (ESMs) that
161 incorporate fire components (Hantson et al., 2016; Hantson et al., 2020). In addition, recent global reconstructions of fire
162 activity designed to support modelling applications have likewise adopted grid-based datasets at monthly resolution (Guo et
163 al., 2025; Williams et al., 2026).

164 Before calculating gsumFRP, we applied three quality filters to minimise errors associated with scan geometry and thermal
165 source types (Li et al., 2018; Chen et al., 2023): we only used AF pixels with confidence level $\geq 30\%$, thermal type equal to 0
166 (vegetation fire), a positive FRP value, and scan angle $\leq 24^\circ$ to reduce geolocation errors (Li et al., 2018). Next, we calculated
167 the sum of the FRP values of the remaining AFs in each CME.

168 **2.3 Geographic division of the world**

169 Fire occurrence and its characteristics vary across the world in terms of size, frequency, intensity and seasonality, in patterns
170 of activity that are commonly known as fire regimes or pyromes (Archibald et al., 2013). Consequently, the geographical
171 division of the world used to explore fire dynamics will influence the identification of EFEs (Jones et al., 2024; Kelley et al.,
172 2025). For example, some regions like the tropical and subtropical savannas present much higher burned areas than other
173 regions (Andela et al., 2017), while individual fires tend to be large and long-lasting in boreal regions (Andela et al., 2019).
174 Similarly, some areas present higher fire intensities (i.e., FRP values) than others (Cunningham et al., 2024, 2025b). Therefore,
175 identifying EFEs by comparing fire metrics within a geographical area with similar fire characteristics can reduce the potential
176 problems of global biases. Because we aim to create a database of CME that can be considered extreme in different areas of
177 the world, we used a geographical reference 55 regions based on the global biomes proposed by Dinerstein et al. (2017),
178 subdivided by continent to better capture the social, ecological, and climatic heterogeneity leading to different fire regimes.
179 Continental biomes with an area equal to or less than 125,000 km² were merged with ecologically or geographically close
180 regions. We also merged the Mediterranean ecosystems of Europe, Western Asia, and Northern Africa, thus creating an
181 independent region for the Southern African Mediterranean biome. Further, we divided the African and South American
182 savannas and deserts into their northern and southern hemisphere regions. Hereafter, we refer to these regions as modified
183 continental biomes (MCBs, see a complete description of these regions, including their names, delimitation criteria, and
184 location in Table S1, and their geographical distribution in Fig. 2).

185 All 0.25° grid cells and FRY fire perimeters were assigned to an MCB according to their geographical location. When a grid
186 cell or fire perimeter overlapped with more than one MCB, it was assigned to the MCB with the largest area overlap. EFEs
187 were identified on a per-MCB basis. This approach made it possible to minimise the underestimation of EFE identification in
188 biomes that present fire regimes with typically smaller burned areas and lower intensities, and the overestimation of EFE
189 identification in others.



190

191 **Figure 2: Delimitation of the 55 modified continental biomes (MCBs) used for the classification of extreme fire events (EFEs) at a**
192 **global scale. Each polygon represents a unique combination of biome and continent, with a region identifier (ID) from 1 to 55 (see**
193 **Table S1 for a complete definition). This regionalization is based on Dinerstein et al. (2017) global biomes, adapted and delimited at**
194 **the continental level with some additional modifications.**

195 2.4 Identification of EFEs

196 EFEs were identified by the gBA and gsumFRP values using a standardisation approach (based on standard deviations from
197 the mean), that aimed to separate normal and extreme fire activity. This approach is commonly employed in the literature to
198 detect climatic and ecological anomalies. This method has been applied in different contexts, adjusting the standardization to
199 the variable of interest, for example, to detect anomalies in vegetation cover using the Normalised Difference Vegetation Index
200 (NDVI) (Yool, 2001; Peters et al., 2002), or to gauge anomalous fire seasons in terms of BA and fire counts (number of AFs)
201 in comparison to previous fire seasons (Jones et al., 2024; Kelley et al., 2025). It has also been applied to define extreme daily
202 fires based on deviations from the regional average of the area burned daily (Balik et al., 2024), to assess daily fire spread rates
203 and their relationship to fire occurrence patterns at the landscape scale (McFarland et al., 2025), and also to characterize
204 precipitation anomalies using the Standardised Precipitation Index (SPI) with the same standardization approach (McKee et
205 al., 1993).

206 In our analysis, we first applied a logarithmic transformation to each gBA and gsumFRP values to normalise the input variables,
207 as they present a skewed distribution. Then, for each variable and MCB separately, we calculated the Z scores for each CME,
208 which was considered extreme if both transformed variables (gBA and gsumFRP) exceeded 2 standard deviations from the
209 regional MCB mean. In other words, EFEs were defined as events that simultaneously present large BA and high FRP values.



210 This requirement of simultaneity in extreme values is referred to in this paper as the $gBA+gsumFRP$ criterion. This approach
211 was adopted to provide a more comprehensive definition of extreme events: while FRP reflects fire intensity, BA reflects fire
212 extent, and both aspects are relevant to assessing anomalous fire impacts within a given biome. Previous studies (e.g., Bowman
213 et al., 2017; Cunningham et al., 2024) typically consider only one variable, but we consider it essential to incorporate both to
214 better capture the full scope of EFEs.

215 As mentioned previously, we complemented the CME analysis by evaluating fire perimeters from the FRY database to identify
216 those with extreme characteristics. Fire perimeters presenting extreme characteristics were identified using the same
217 standardised anomaly approach applied to CMEs evaluating each of the FRY fire variables (size, duration, median FRP, rate
218 of spread, or severity) independently. Before calculating the anomalies, all fire perimeter variables were log-transformed to
219 reduce skewness. While CMEs were classified as extreme based on the combined $gBA+gsumFRP$ criterion, the EFE database
220 incorporated dedicated fields to indicate whether an extreme CME was also overlapping an extreme fire perimeter, using any
221 of the five FRY variables to allow database users to select and explore which variable or combination of variables to use when
222 studying EFEs. For doing that, each fire perimeter identified as extreme for at least one FRY variable was projected onto the
223 grid, identifying the EFEs with which it overlapped. Next, the temporal component was considered, associating a fire perimeter
224 with an EFE if the duration of the perimeter overlapped temporally, even partially, with the corresponding month. For example,
225 the information of a fire perimeter identified as extreme with a duration from September 23 to November 16, 2009, would be
226 assigned to the spatially overlapping EFEs of September, October, and November of that year.

227 When an EFE overlapped with one or more fire perimeters with extreme characteristics, the variables for which those
228 perimeters were classified as extreme were recorded as binary descriptors of the corresponding EFE (1 = extreme, 0 = not
229 extreme).

230 The final database therefore integrates, for each CME, its classification as an extreme fire according to the combined
231 $gBA+gsumFRP$ criterion, together with information derived from FRY perimeters specifying which variables were extreme
232 within the same spatial and temporal boundaries. This structure preserves CMEs as the principal spatial unit of analysis while
233 using fire perimeters as complementary information that provide additional context on the extreme CME.

234 **3 Results**

235 **3.1 Structure of the EFEs database**

236 EFEs database (Solano-Romero and Segura-Garcia, 2025) consists of a set of NetCDF files, corresponding to each month of
237 the period 2003-2022. The files use the WGS84 geographic coordinate system and are systematically named according to the
238 year and month of the record (i.e., *EFEs_dataset_<year><month>.nc*).

239 Each file contains 11 layers comprising information on extreme fires (Table 1). The main layer (*efes_id*) classifies each CME
240 into three categories: 0, no fire activity; 1, CME identified as EFE according to the combined criterion $gBA+gsumFRP$; and 2,
241 CME with fire activity ($gBA > 0$ and/or $gsumFRP > 0$) but not considered extreme under this criterion. In addition, seven



242 additional layers are included indicating whether any of the gBA, gsumFRP or the five FRY variables were classified as
 243 extreme for each grid cell in that particular month. These layers indicate whether each grid cell presented extreme gBA or
 244 gsumFRP values (coded as 1 if extreme values, and otherwise as 0); and whether it overlaps (1, otherwise 0) with at least one
 245 extreme patch for each variable.

246 The files also include three additional layers, which provide basic information for each CME: *burned_area*, which indicates
 247 the total BA (gBA, in m²); *sum_frp*, which represents the sum of the filtered FRP values (gsumFRP, in MW) and *region_ID*,
 248 an integer from 0 to 55 that identifies the MCB region to which the cell belongs (Table S1).

249
 250 **Table 1: Description of the layers included in the extreme fire events (EFEs) database, covering the period 2003 to 2022. The main**
 251 **layer, efes_id, identifies whether a cell-month event (CME) had fire activity and whether it was classified as an EFE according to**
 252 **combined criteria of burned area (gBA) and total radiative power (gsumFRP). Layers with the prefix efes_FRY represent the**
 253 **different characteristics of extreme events, such as size, median FRP, rate of spread, severity, and duration, according to the extreme**
 254 **fire perimeters. Other layers provide information on the total burned area, total FRP, and the modified continental biomes (MCBs)**
 255 **region assigned to each CME.**

Extreme Fire Events (EFEs) Database	
Format	NetCDF
EPSG	4326
Spatial Resolution	0.25°
Time Period	2003-2022 - Monthly.
Statistical method of analysis	Two standard deviations on the logarithm of the variables.
Layer name	Description
efes_id	Main layer. Indicates whether the CME showed any fire activity and whether it was classified as extreme based on the combined gBA and gsumFRP criteria: <ul style="list-style-type: none"> • 0: no fire activity (gBA = 0 and gsumFRP = 0). • 1: extreme event, identified because both variables (gBA and gsumFRP) exceeded the threshold simultaneously. • 2: fire activity detected (gBA > 0 and/or gsumFRP > 0), but not classified as extreme because both thresholds were not met simultaneously.
efes_gBA	Binary variable. 1 if the CME was classified as extreme by gBA (derived from the FireCCI51 grid product); 0 otherwise.
efes_gsumFRP	Binary variable. 1 if the CME was classified as extreme by gsumFRP (sum of FRP from MCD14ML); 0 otherwise.
efes_FRYsize	Binary variable. 1 if any FRY fire perimeter identified as extreme by size overlaps with the CME; 0 otherwise.
efes_FRYmedfrp	Binary variable. 1 if any FRY fire perimeter identified as extreme by median FRP overlaps with the CME; 0 otherwise.
efes_FRYros	Binary variable. 1 if any FRY fire perimeter identified as extreme by Rate Of Spread (ROS) overlaps with the CME; 0 otherwise.
efes_FRYseverity	Binary variable. 1 if any FRY fire perimeter identified as extreme by burn severity overlaps with the CME; 0 otherwise.

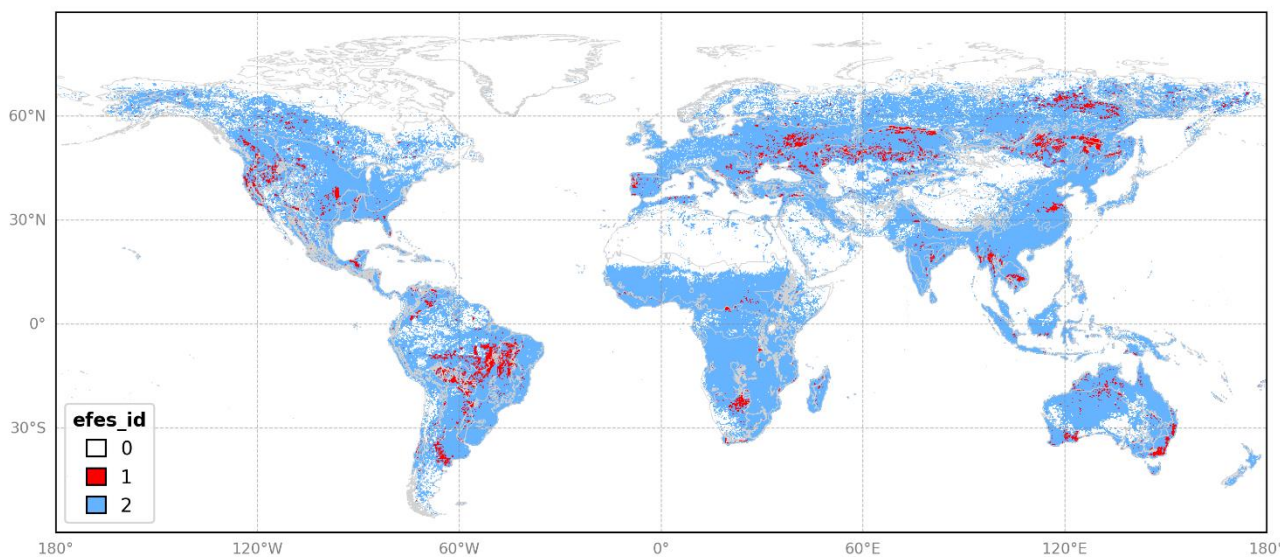


efes_FRyduration	Binary variable. 1 if any FRY fire perimeter identified as extreme by duration overlaps with the CME; 0 otherwise.
burned_area	Total BA (m ²) in the CME (gBA), derived from the FireCCI51 grid product.
sum_frp	Total FRP (MW) in the CME, derived from MCD14ML after filtering certain MODIS active fire detections.
region_ID	Integer from 0 to 55 indicating the modified continental biome the CME belongs to (Table S1).

256

257 **Spatio-temporal analysis of EFes**

258 Figure 3 shows the spatial distribution of CMEs according to the presence of fire activity and their classification as EFes based
 259 on the combined gBA and gsumFRP criterion. EFes were detected in most biomes, with particularly high frequencies in
 260 tropical seasonally dry ecosystems, temperate and boreal forests, and semi-arid grasslands and shrublands. The EFes database
 261 identified 19,951 extreme CMEs during the analysed period (2003-2022). Of these EFes, approximately 96% coincided
 262 spatially and temporally with at least one fire perimeter classified as extreme according to the FRY variables (fire size, duration,
 263 median FRP, ROS or severity). In addition, Figure 4 shows the distribution of events according to the combinations of FRY
 264 variables associated with the EFes. The most frequent combination was that of extremes in fire perimeter duration and size
 265 (27.6%), followed by the combination of duration, ROS and size (20.0%), and by the combination of ROS and size (10.5%).

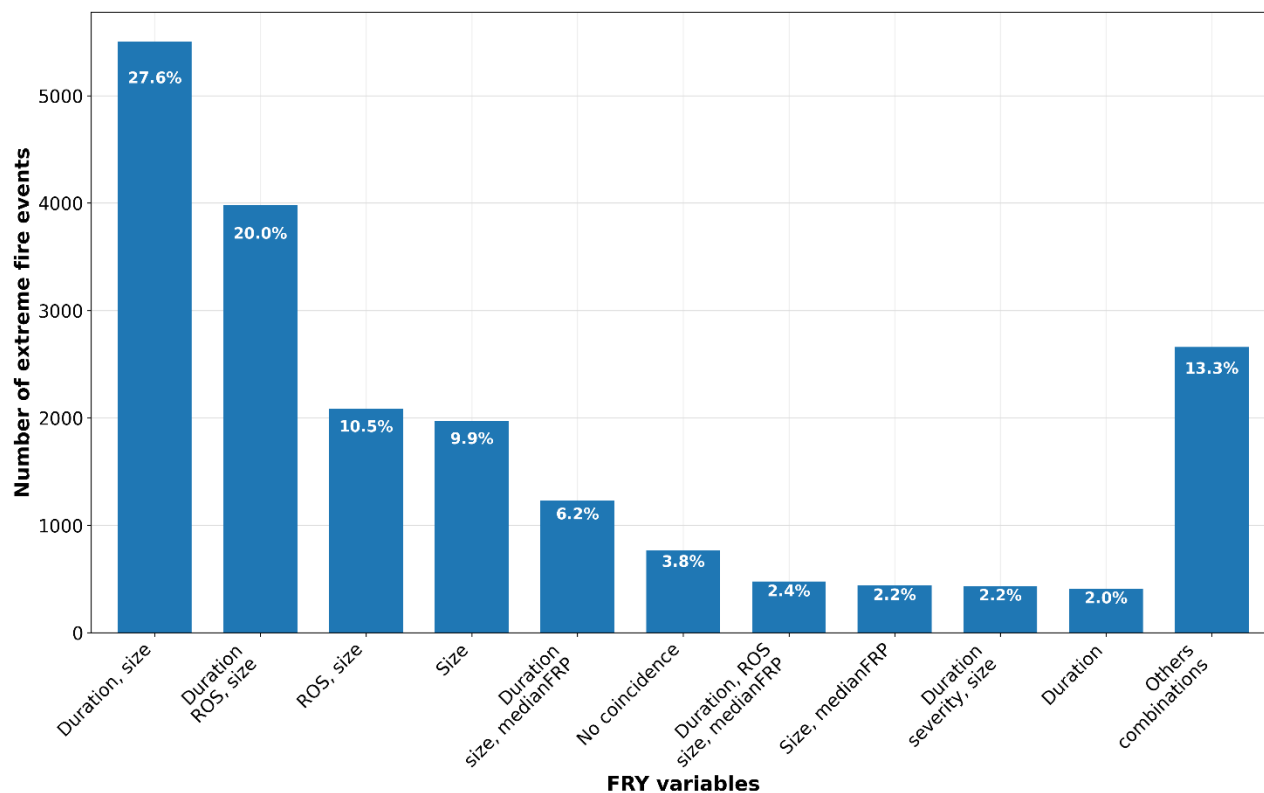


266
 267

268 **Figure 3: Visualization of the efes_id layer for the 2003-2022 time series. Category 0 represents cell-month events (CMEs) with no**
 269 **fire activity during the entire period (in white). Category 1 (in red) corresponds to CMEs identified as extreme fire events (EFes) in**
 270 **at least one month of the series, according to the combined gBA+gsumFRP criterion. Category 2 (in blue) includes CMEs that had**
 271 **fire activity at least once during the period but were not classified as EFes.**



272



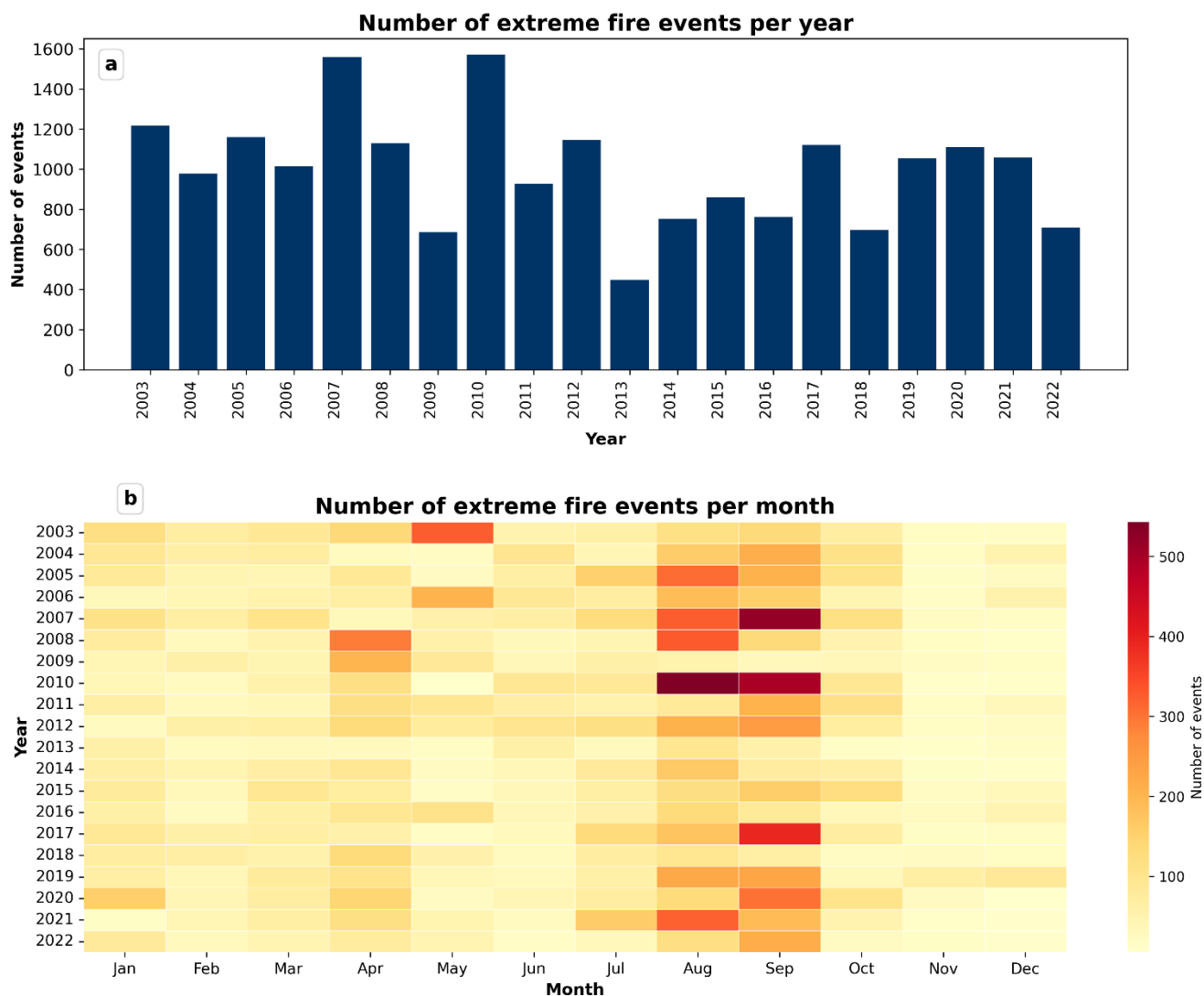
273

274 **Figure 4: Combination of extreme fire events (EFEs) and FRY variables in which fire patches were also identified as extreme. The**
275 **bar chart shows the 10 combinations of variables with the highest number of extreme events, plus an aggregate category called**
276 **‘Other combinations’ that groups all the remaining combinations. The “No coincidence” bar represents the EFEs that did not match**
277 **any extreme FRY variable. The percentages within each bar represent the proportion of events relative to the total number of EFEs.**

278 At the global scale, the EFEs identified in the database showed marked temporal variability (Fig. 5). Specifically, Figure 5a
279 shows that interannual counts varied substantially during 2003-2022, with a mean of 997.5 events per year and no clear
280 temporal trend. The maximum value was recorded in 2010, with 1,572 EFEs, whereas the minimum was observed in 2013,
281 with 448 EFEs. In turn, Figure 5b reflects a well-defined seasonality in the monthly distribution of EFEs. The highest values
282 were concentrated in August and September, which accumulated 3,898 and 4,121 events, respectively, and together accounted
283 for around 40% of the total recorded during the analysed period. At some distance, April ranked third, with 2,120 events,
284 followed by July (1,583) and January (1,434). At the opposite end, November and December showed the lowest cumulative
285 numbers of EFEs, with 400 and 510 events, respectively. This pattern is consistent with the superposition of different seasonal
286 fire regimes at the global scale. In particular, the predominance of events in late boreal summer is consistent with the high fire



287 activity observed across extensive temperate and boreal regions of the Northern Hemisphere, while also coinciding with the
288 dry season in several tropical and subtropical regions of the Southern Hemisphere, as shown by the spatial patterns described
289 by Lizundia-Loiola et al. (2020).



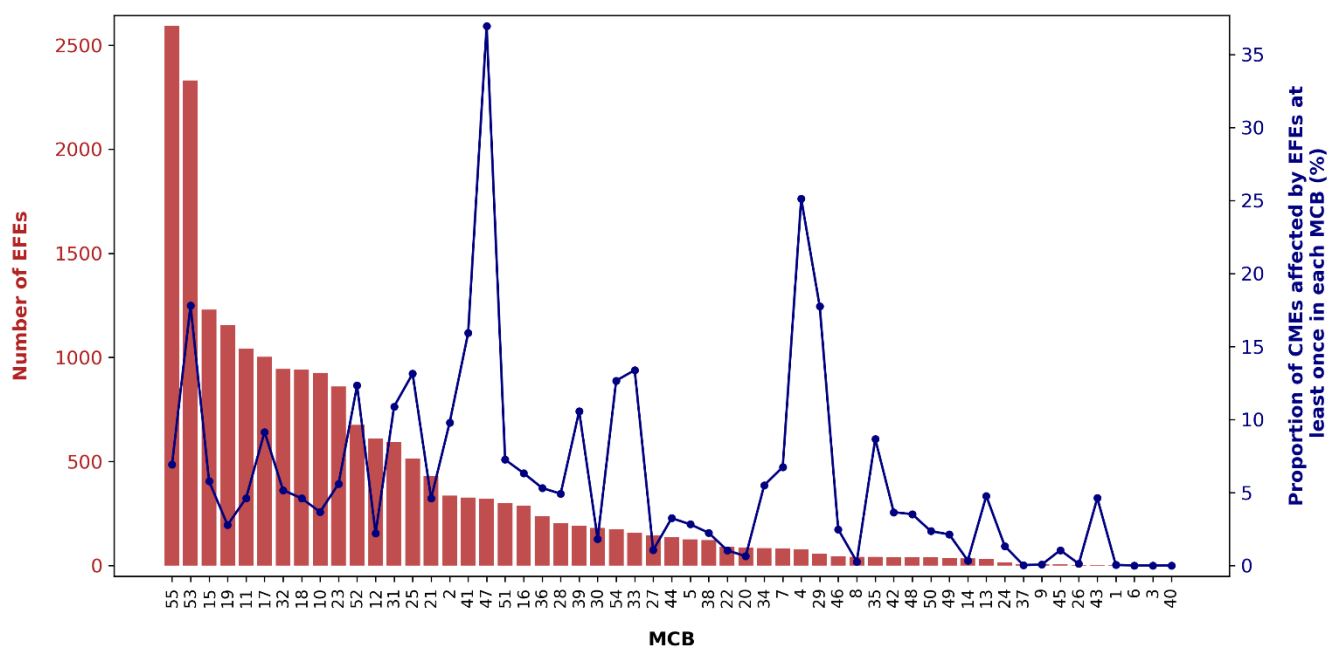
290

291 **Figure 5: Number of extreme fire events (EFEs) identified in the database. Panel (a) shows the annual total of EFEs globally. Panel**
292 **(b) shows the global monthly number of EFEs.**

293 The distribution of EFEs across continental biomes was highly uneven (Fig. 6). Of the 55 continental biomes considered, 52
294 recorded at least one EFE during the study period, while only three did not present any extreme event: Africa-Flooded
295 Grasslands & Savannas (ID 3), Africa-Temperate Broadleaf & Mixed Forests (ID 6), and Australia-Oceania-Montane
296 Grasslands & Shrublands (ID 40). Approximately 50% of all EFEs were concentrated in just six regions. The largest



297 contributions corresponded to South America-Tropical & Subtropical Moist Broadleaf Forests (ID 55) and South America-
298 Tropical & Subtropical Grasslands, Savannas & Shrublands-Southern Hemisphere (ID 53), with 2,591 and 2,331 EFEs,
299 respectively (Fig. 6). These were followed by several Asian biomes, in particular Asia-Temperate Broadleaf & Mixed Forests
300 (ID 15), Asia-Tropical & Subtropical Moist Broadleaf Forests / Mangroves / Tropical & Subtropical Grasslands, Savannas &
301 Shrublands (ID 19), and Asia-Boreal Forests/Taiga (ID 11), together with Asia-Temperate Grasslands, Savannas & Shrublands
302 (ID 17) and North America-Temperate Grasslands, Savannas & Shrublands (ID 32). In contrast, 30 regions contributed less
303 than 10% of the total EFEs, reinforcing the idea that the occurrence of extreme events is strongly concentrated in a limited
304 number of continent-biome combinations (See Fig. S2 for a spatial interpretation of the number of EFEs by MCB). However,
305 this pattern changes when considering the proportion of CMEs that were affected by at least one EFE within each MCB. From
306 this perspective, the highest values corresponded to South America-Flooded Grasslands & Savannas (ID 47), with 37% of its
307 CMEs affected at least once, and Africa-Mediterranean Forests, Woodlands & Scrub-Southern Hemisphere (ID 4), with 25%.
308 South America-Tropical & Subtropical Grasslands, Savannas & Shrublands-Southern Hemisphere (ID 53) and North America-
309 Mediterranean Forests, Woodlands & Scrub (ID 29) also stood out, with 18% in both cases. At a second level, Australia /
310 Oceania-Temperate Broadleaf & Mixed Forests / Montane Grasslands & Shrublands (ID 41) reached 16%. This shows that
311 the absolute number of EFEs and their relative spatial extent do not always coincide.
312



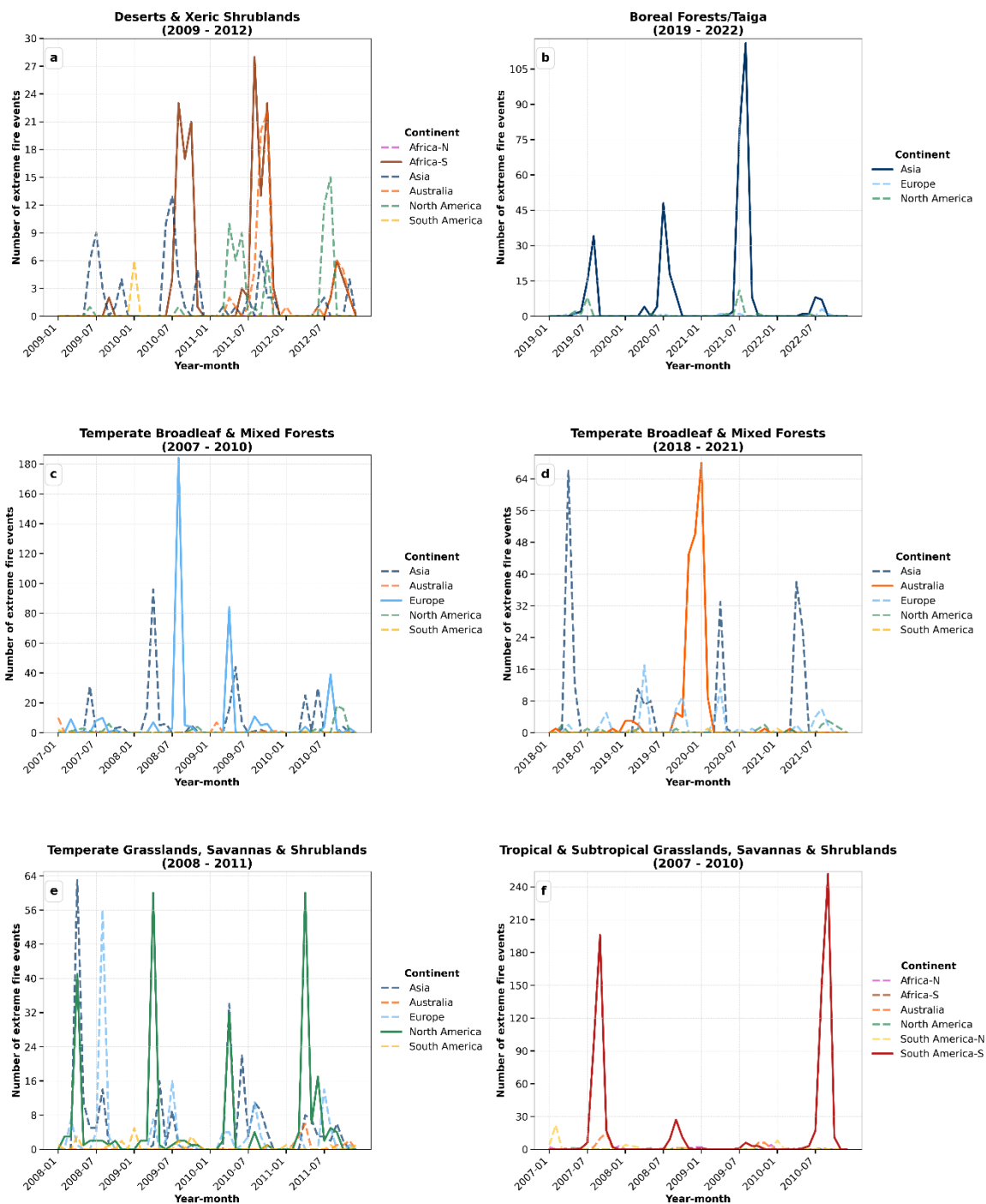
313
314 **Figure 6: Number and proportion of extreme fire events (EFEs) per modified continental biomes (MCB). Bars**
315 **represent the total number of EFEs in each MCB across the entire time series, including repeated occurrences in the**



316 **same cells, while the line shows the proportion of cell-month events (CMEs) that have been classified as EFEs at least**
317 **once in each MCB.**

318

319 At the continental scale, the temporal distribution of EFEs showed marked differences among biomes and regions (Fig. 7).
320 Each panel represents the biome and the period in which a given continent recorded the highest concentration of EFEs. The
321 solid line identifies the continent with the greatest number of EFEs in that biome during the study period, while the dashed
322 lines correspond to the remaining continents. In Africa, the highest concentration of EFEs was recorded in the Deserts & Xeric
323 Shrublands biome, mainly in the Southern Hemisphere, with notable peaks in August 2010 and August 2011 (Fig. 7a). In Asia,
324 the most prominent biome was Boreal Forests/Taiga, where a very pronounced peak was observed in August 2021, clearly
325 exceeding those recorded in other continents sharing this biome (Fig. 7b). In Europe and Australia, the most affected biome
326 was Temperate Broadleaf & Mixed Forests, although during different periods. In Europe, the highest EFE activity was
327 concentrated between 2007 and 2010, with particularly intense peaks in August 2008 and a second relevant maximum in 2009
328 (Fig. 7c). In contrast, in Australia, peak activity in this same biome occurred between 2018 and 2021, with a very strong
329 concentration of events between November and December 2019 and January 2020 (Fig. 7d). In North America, the highest
330 number of EFEs was recorded in the Temperate Grasslands, Savannas & Shrublands biome, with well-defined peaks in April
331 2009 and April 2011 (Fig. 7e). Finally, in South America, the highest concentration of extreme events was observed in Tropical
332 & Subtropical Grasslands, Savannas & Shrublands, particularly in the Southern Hemisphere, with very pronounced maxima
333 in September 2007 and September 2010 (Fig. 7f).



334

335

336

Figure 7: Biome and time interval in which a continent recorded the highest concentration of extreme fire events (EFEs). Within each panel, the lines represent the monthly evolution of the number of EFEs. The solid line indicates

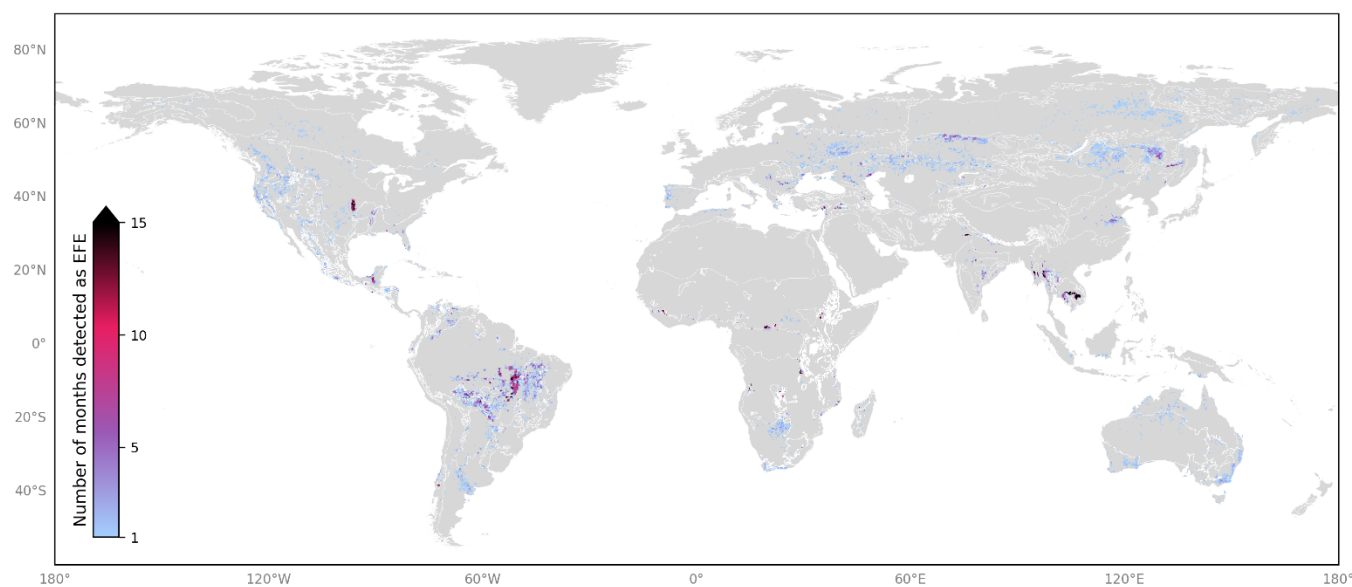


337 **the continent that recorded the highest number of EFEs, while the dashed lines correspond to the remaining continents.**
338 **The labels -N and -S indicate the subdivision of some continents into the Northern and Southern Hemispheres,**
339 **respectively.**

340 This temporal variability across continents and biomes is accompanied by a clear pattern of spatial recurrence in extreme fire
341 activity (Fig. 8). Based on the frequency with which each grid cell was identified as extreme, distinct recurrence patterns
342 emerge at the global scale. A limited number of cells exhibited high recurrence, with EFEs recorded in more than 15 different
343 years over the study period. These recurrent EFEs tend to show higher annual values of gBA and gsumFRP than other non-
344 recurrent EFEs, and other CMEs in the same MCB that were not classified as extreme according to the gBA+gsumFRP
345 criterion (Fig. S3 and Fig. S4).

346 Furthermore, we found that fire activity frequency (defined as the number of months in which a CME exhibited any fire
347 activity) is consistently among the highest in cells with recurrent EFEs, compared to all grid cells that experienced fire at any
348 point (Fig. S5). Specifically, EFEs recorded over a period of 15 years or more tend to exhibit more frequent fire activity and,
349 overall, higher intensity than other cells within the same MCB. Recurrent EFEs were mainly observed in landscapes with low
350 levels of transformation, where high levels of non-extreme fire activity are also commonly recorded, as is the case, for example,
351 in Temperate Grasslands, Savannas & Shrublands in North America. However, recurrent EFEs were also detected in highly
352 anthropised landscapes, such as Deserts & Xeric Shrublands in some regions of Asia.

353



354

355 **Figure 8: Monthly spatial distribution of the frequency of extreme fire events (EFEs) during the period 2003-2022. The colors**
356 **represent the number of months in which at least one EFE was recorded in each cell-month events (CMEs). CMEs with no**



357 **detected EFEs are shown in gray color. The color scale is visually limited to 15 events; however, the actual maximum frequency**
358 **reaches 30. Values above 15 are represented with the maximum color intensity.**

359 **3.2 Intercomparison analysis**

360 Given that there is no pre-existing global database of extreme fires, and a lack of consensus in the literature on the definition
361 of ‘extreme fire’ to validate our product, we compared our database against a list of events that we have identified in the
362 scientific literature. We conducted the search in Google Scholar using the following combinations of keywords: ‘extreme
363 wildfire events’, ‘megafires’, ‘large fire events’, ‘catastrophic wildfires’, along with terms related to the climate and
364 environmental context (‘fire behaviour’, ‘fire season’, ‘climate change’, ‘carbon emissions’ and ‘satellite-derived burned
365 area’). We also included in our search the names of affected regions, such as Australia, Amazonia, Canada, Chile, Portugal,
366 Indonesia, Siberia and the United States, to ensure a globally representative coverage of extreme fires.

367 We selected twenty representative events (Table S2) that documented large-scale fires in different ecosystems, climatic and
368 socio-economic contexts within the study period. To assess whether these events were present in our EFE database, we
369 compared the geographic area described in each article with the records in the database. An event was considered mapped if it
370 coincided with the reported location and with the same months in the database.

371 Using this procedure, the EFE database identified 18 of the 20 EFEs identified in the literature, which include some of the
372 worst fire events on record in the last decades, such as the Black Summer in Australia (2019-2020), Amazonia (2019), Canada
373 (2014), Chile (2017), Portugal (2003 and 2017), Indonesia (2015), Siberia (2003 and 2021) and the western United States
374 (2018 and 2020). The two events that were not detected by our database were the Mati fire (Greece, 2018) and the Marshall
375 fire (Colorado, 2021). The Mati fire, which occurred in July 2018, caused the deaths of 103 people and the destruction of some
376 4,000 homes, as well as thousands of vehicles (Bitek and Erenoğlu, 2022). The Marshall fire, in December 2021, originated in
377 the state of Colorado (USA) and was notable for its rapid spread, driven by winds of up to 160 km/h, which caused the
378 destruction of more than 1,000 homes and significant economic damage (Benjamin et al., 2023; Balch et al., 2024). In both
379 cases, fires were highly destructive in terms of human and material impact, but relatively small in size, extending over
380 approximately 1,500 ha in Mati (Bitek and Erenoğlu, 2022) and 2,400 ha in Marshall (Benjamin et al., 2023). At a spatial
381 resolution of 0.25°, these areas represent a very small fraction of a grid cell, probably explaining why we did not identify them
382 as extreme events according to our identification criteria.

383 The EFE database presented here provides an assessment of extreme events based on their size and energy release. However,
384 the social impacts of fires are not always linked to these characteristics, but rather to where and when fires occur, particularly
385 when happening in the vicinity of densely populated areas (Teymoor Seydi et al., 2025). The difficulty of obtaining consistent
386 global-scale information on the social impacts of fires restricts the conceptualization and posterior identification of extreme
387 fire events in relation to these impacts; while fire variables associated with fire activity and behaviour can be approached from
388 satellite datasets across space and time. Still extreme socio-economic impacts from fire are of course a subject of paramount
389 importance and need to be evaluated whenever consistent data are available.



390 4 Data and code availability

391 EFES database is publicly available in the Consorcio Madroño repository under the main folder
392 *Extreme_Fire_Events_EFES_database*, which contains the subfolder *EFES_dataset_2003-2022* with the full database
393 (<https://edatos.consorcioadrono.es/previewurl.xhtml?token=94b577ad-c940-4042-9a4e-239102294a4e>, Solano-Romero
394 and Segura-Garcia, 2025).

395 The compilation of the EFES dataset was based on three external data inputs, all of which are publicly available. The **Fire_cci**
396 **Burned Area v5.1 (FireCCI51) grid product** is available at the European Space Agency Climate Change Initiative. CEDA
397 Catalogue: <https://catalogue.ceda.ac.uk/uuid/3628cb2fdb443588155e15dee8e5352/> Period: 2001-2022. Last accessed: 9
398 October 2025 (European Space Agency, 2025b). The global database of fire patch functional traits **FRY version 2.0**
399 (**provisional**) is available at OSF repository: <https://osf.io/rjvz5/>. Last accessed: 9 October 2025 (Chen, 2025). Finally,
400 **MCD14ML Active Fire Product (MODIS)** was accessed through the University of Maryland SFTP server (FUOCO). Last
401 accessed: 9 October 2025 (University of Maryland, 2020).

402 All datasets are open access and can be freely downloaded from their respective repositories.

403 The codes used for the development of the EFES database (Solano-Romero and Segura-Garcia, 2025) are freely available in
404 the Consorcio Madroño repository under the main folder *Extreme_Fire_Events_EFES_database*, which contains the subfolder
405 *Codes* with all scripts used for data processing and analysis, in line with the FAIR Guiding Principles (Wilkinson et al., 2016).

406 5 Discussion and conclusions

407 EFES database presented here represents, to the best of our knowledge, the first global dataset specifically designed to
408 characterize extreme fire activity. Developed under the ESA Climate Change Initiative (CCI) as part of the XFires project, the
409 database contributes to the project's goal of improving the understanding of extreme fires and their environmental impacts by
410 providing essential data for climate modelers. While previous studies have addressed extreme fires at global scales (e.g.,
411 Bowman et al., 2017; Cunningham et al., 2024), they have generally relied on a single metric, such as cell-level FRP
412 (Cunningham et al., 2024), without explicitly accounting for the variability of fire regimes across different biomes. In this
413 context, the EFES database provides a novel approach by combining BA and FRP with additional descriptive variables derived
414 from fire perimeters and by using continental biomes as the geographical reference framework for characterizing extremes.
415 This dataset enables a more comprehensive representation of extreme fire activity and broadens its utility both for analyzing
416 historical patterns during the reference period and for incorporation as predictive variables in Earth System Models (ESMs),
417 Dynamic Global Vegetation Models (DGVMs), and other meteorological, emission, and global fire models.

418 The selection of FireCCI51 as the burned area data source was guided not only by considerations of data quality and temporal
419 consistency, but also by the methodological framework within which this database has been developed, closely linked to the
420 products generated under ESA's CCI projects. From this perspective, the priority was to define a robust, homogeneous, and
421 methodologically stable reference period on which extreme events could be characterized consistently across regions and



422 biomes. Global accuracy assessments indicate that FireCCI51 presents lower omission errors between 2017 and 2019 than
423 alternative products such as MCD64A1 (Franquesa et al., 2022), with global Dice Coefficient values for these three years of
424 66.7% for FireCCI51 compared to 62.5% for MCD64A1, making it a more reliable source for detecting extreme events over
425 long time series. However, because FireCCI51 is based on MODIS data and the more recent development of the FireCCI
426 project has led to a new burned area product based on Sentinel-3, FireCCIS311 (Lizundia-Loiola et al., 2022), a consistency
427 issue arises between the two series. In particular, FireCCI51 and FireCCIS311 do not detect exactly the same burned area,
428 meaning that a direct extension of the EFES database beyond 2022 could introduce artificial discontinuities in the identification
429 and characterization of extreme events. For this reason, this study limited the database to the 2003–2022 period, defined from
430 a single burned area source and therefore internally consistent for the comparison of extremes across regions and biomes.
431 Future advances in the harmonization of both products may facilitate the extension of this database to more recent periods
432 without compromising the consistency of the reference framework. In addition, we used FRY v2.0 for the EFES database
433 because it provides detailed descriptive metrics and, by using the version derived from the FireCCI51 burned area product,
434 ensures consistency in temporal coverage, allowing fire perimeters-level and cell-level analyses to be comparable across the
435 reference period.

436 The use of the EFE database can provide valuable insights into the typology of EFES, thus complementing the analysis being
437 currently conducted on BA and FRP trends (Kelley et al., 2025; Abatzoglou et al., 2025; Ghasemiazma et al., 2026). Some
438 EFES are identified as extreme recurrently, which reflects the high variability of fire activity within certain MCBs. These areas
439 contain CMEs with much higher and more recurrent fire activity than others. As a result, these EFES are almost annually
440 classified as extreme relative to the surrounding cells, rather than necessarily indicating a particular ecological or land
441 management pattern. This methodological characteristic should be considered when interpreting spatial patterns in the database
442 or performing regional comparisons. The analysis of the EFE database, along with climate, vegetation and socio-economic
443 drivers may provide new explanation models on the drivers leading these types of extreme anomalies.

444 Overall, the EFES database represents a novel and useful tool for the study of EFES at global scales. Its combination of
445 complementary fire variables, cell-month temporal resolution, and integration with fire perimeter-level descriptors allows for
446 detailed characterisation of extreme events while maintaining consistent global coverage. This resource will support modelers,
447 ecosystem studies, and fire management applications by providing a standardised reference of extreme fire activity from 2003
448 to 2022.

449
450
451
452
453



454 **Supplement link**

455 Supplementary material is attached

456

457 **Author contributions**

458 ESR: Conceptualization, Methodology, Software, Analysis, Data curation, Investigation, Validation, Writing - original draft,
459 Writing - review and editing. CSG: Conceptualization, Methodology, Software, Analysis, Data curation, Investigation, Writing
460 - review and editing. MLP: Conceptualization, Project administration, Writing - review and editing. AK: Conceptualization,
461 Writing - review and editing. MÁTV: Conceptualization, Writing - review and editing. ECh: Supervision, Project
462 administration, Conceptualization, Writing - review and editing, Funding acquisition.

463 **Competing interest**

464 The authors declare no competing interests

465

466 **Disclaimer**

467 Publisher's note: Copernicus Publications remains neutral with regard to jurisdictional claims made in the text, published
468 maps, institutional affiliations, or any other geographical representation in this paper. While Copernicus Publications makes
469 every effort to include appropriate place names, the final responsibility lies with the authors. Views expressed in the text are
470 those of the authors and do not necessarily reflect the views of the publisher

471

472 **Acknowledgements**

473 We thank the Environmental Remote Sensing Research Group (GITA) at the Universidad de Alcalá (Spain) and the partners
474 at the XFires project (funded by the European Space Agency) for helpful feedback during discussions of this project

475

476 **Financial support**

477 This study was funded by the European Space Agency (ESA) XFires project, contract N° 4000145352/24/I-LR.

478 **References**

479 Abatzoglou, J. T., Kolden, C. A., Cullen, A. C., Sadegh, M., Williams, E. L., Turco, M., and Jones, M. W.: Climate change
480 has increased the odds of extreme regional forest fire years globally, *Nature Communications*, 16, 6390, 10.1038/s41467-025-
481 61608-1, 2025.



- 482 Abram, N. J., Henley, B. J., Sen Gupta, A., Lippmann, T. J., Clarke, H., Dowdy, A. J., Sharples, J. J., Nolan, R. H., Zhang, T.,
483 and Wooster, M. J.: Connections of climate change and variability to large and extreme forest fires in southeast Australia,
484 *Communications Earth & Environment*, 2, 8, 10.1038/s43247-020-00065-8, 2021.
- 485 Adams, M. A.: Mega-fires, tipping points and ecosystem services: Managing forests and woodlands in an uncertain future,
486 *Forest Ecology and Management*, 294, 250-261, 10.1016/j.foreco.2012.11.039, 2013.
- 487 Alonso-González, E. and Fernández-García, V.: MOSEV: a global burn severity database from MODIS (2000–2020), *Earth
488 System Science Data*, 13, 1925-1938, 10.5194/essd-13-1925-2021, 2021.
- 489 Andela, N., Morton, D. C., Giglio, L., Paugam, R., Chen, Y., Hantson, S., Van Der Werf, G. R., and Randerson, J. T.: The
490 Global Fire Atlas of individual fire size, duration, speed and direction, *Earth System Science Data*, 11, 529-552, 10.5194/essd-
491 11-529-2019, 2019, 2019.
- 492 Andela, N., Morton, D. C., Giglio, L., Chen, Y., van der Werf, G. R., Kasibhatla, P. S., DeFries, R. S., Collatz, G., Hantson,
493 S., and Kloster, S.: A human-driven decline in global burned area, *Science*, 356, 1356-1362, 10.1126/science.aal4108, 2017.
- 494 Archibald, S. and Roy, D.: Identifying individual fires from satellite-derived burned area data, 2009 IEEE International
495 Geoscience and Remote Sensing Symposium, Cape Town, South Africa, III-160-III-163, 10.1109/IGARSS.2009.5417974,
496 Archibald, S., Lehmann, C. E., Gómez-Dans, J. L., and Bradstock, R. A.: Defining pyromes and global syndromes of fire
497 regimes, *Proceedings of the National Academy of Sciences*, 110, 6442-6447, 10.1073/pnas.1211466110, 2013.
- 498 Balch, J. K., Iglesias, V., Mahood, A. L., Cook, M. C., Amaral, C., DeCastro, A., Leyk, S., McIntosh, T. L., Nagy, R. C., and
499 St. Denis, L.: The fastest-growing and most destructive fires in the US (2001 to 2020), *Science*, 386, 425-431,
500 10.1126/science.adk5737, 2024.
- 501 Balik, J. A., Coop, J. D., Krawchuk, M. A., Naficy, C. E., Parisien, M.-A., Parks, S. A., Stevens-Rumann, C. S., and Whitman,
502 E.: Biogeographic patterns of daily wildfire spread and extremes across North America, *Frontiers in Forests and Global
503 Change*, 7, 1355361, 10.3389/ffgc.2024.1355361, 2024.
- 504 Bell, J. E., Brown, C. L., Conlon, K., Herring, S., Kunkel, K. E., Lawrimore, J., Luber, G., Schreck, C., Smith, A., and Uejio,
505 C.: Changes in extreme events and the potential impacts on human health, *Journal of the Air & Waste Management
506 Association*, 68, 265-287, 10.1080/10962247.2017.1401017, 2018.
- 507 Benjamin, S. G., James, E. P., Szoke, E. J., Schlatter, P. T., and Brown, J. M.: The 30 December 2021 Colorado Front Range
508 windstorm and Marshall Fire: Evolution of surface and 3D structure, NWP guidance, NWS forecasts, and decision support,
509 *Weather and Forecasting*, 38, 2551-2573, doi.org/10.1175/WAF-D-23-0086.1, 2023.
- 510 Beverly, J. L. and Schroeder, D.: Alberta's 2023 wildfires: context, factors, and futures, *Canadian Journal of Forest Research*,
511 55, 1-19, 10.1139/cjfr-2024-0099, 2024.
- 512 Bitek, D. and Erenoglu, R. C.: Forest Fire Analysis with Sentinel-2 Satellite Imagery: The Case of Mati (Greece) in 2018,
513 *Academic Platform Journal of Natural Hazards and Disaster Management*, 3, 85-98, 10.52114/apjhad.1211651, 2022.
- 514 Bowman, D. M., Kolden, C. A., Abatzoglou, J. T., Johnston, F. H., van der Werf, G. R., and Flannigan, M.: Vegetation fires
515 in the Anthropocene, *Nature Reviews Earth & Environment*, 1, 500-515, 10.1038/s43017-020-0085-3, 2020a.



- 516 Bowman, D. M., Williamson, G. J., Abatzoglou, J. T., Kolden, C. A., Cochrane, M. A., and Smith, A. M.: Human exposure
517 and sensitivity to globally extreme wildfire events, *Nature ecology & evolution*, 1, 0058, 10.1038/s41559-016-0058, 2017.
- 518 Bowman, D. M., Williamson, G., Yebra, M., Lizundia-Loiola, J., Pettinari, M. L., Shah, S., Bradstock, R., and Chuvieco, E.:
519 Wildfires: Australia needs national monitoring agency, *Nature*, 584, 188-191, 10.1038/d41586-020-02306-4, 2020b.
- 520 Chen, W.: FRY version 2.0 provisional, OSF [dataset], 2025.
- 521 Chen, Y., Hall, J., van Wees, D., Andela, N., Hantson, S., Giglio, L., van der Werf, G. R., Morton, D. C., and Randerson, J.
522 T.: Multi-decadal trends and variability in burned area from the fifth version of the Global Fire Emissions Database (GFED5),
523 *Earth System Science Data*, 15, 5227-5259, 10.5194/essd-15-5227-2023, 2023.
- 524 Chuvieco, E., Pettinari, M. L., Lizundia Loiola, J., Storm, T., and Padilla Parellada, M.: ESA Fire Climate Change Initiative
525 (Fire_cci): MODIS Fire_cci Burned Area Grid product, version 5.1 (5.1), Centre for Environmental Data Analysis (CEDA)
526 [dataset], 10.5285/3628cb2fdb443588155e15dee8e5352, 2019.
- 527 Chuvieco, E., Aguado, I., Salas, J., García, M., Yebra, M., and Oliva, P.: Satellite remote sensing contributions to wildland
528 fire science and management, *Current Forestry Reports*, 6, 81-96, 10.1007/s40725-020-00116-5, 2020.
- 529 Cunningham, C., Williamson, G. J., Abatzoglou, J., Kolden, C., Jones, M. W., Fromm, M., Peterson, D. A., Tedim, F.,
530 Flannigan, M., and Johnston, F. H.: Pyrogeography of extraordinary wildfires, 10.31223/X5T187, 2025a.
- 531 Cunningham, C. X., Williamson, G. J., and Bowman, D. M.: Increasing frequency and intensity of the most extreme wildfires
532 on Earth, *Nature ecology & evolution*, 8, 1420-1425, 10.1038/s41559-024-02452-2, 2024.
- 533 Cunningham, C. X., Williamson, G. J., and Bowman, D. M.: Reply to: Increases in the world's most extreme wildfire events
534 probably driven by fire size and simultaneity, *Nature Ecology & Evolution*, 1-4, 10.1038/s41559-025-02742-3, 2025b.
- 535 Desyatkin, A., Okoneshnikova, M., Fedorov, P., Ivanova, A., Filippov, N., and Desyatkin, R.: The Impact of catastrophic
536 forest fires of 2021 on the light soils in Central Yakutia, *Land*, 13, 1130, 10.3390/land13081130, 2024.
- 537 Dinerstein, E., Olson, D., Joshi, A., Vynne, C., Burgess, N. D., Wikramanayake, E., Hahn, N., Palminteri, S., Hedao, P., and
538 Noss, R.: An ecoregion-based approach to protecting half the terrestrial realm, *BioScience*, 67, 534-545,
539 10.1093/biosci/bix014, 2017.
- 540 Duane, A., Castellnou, M., and Brotons, L.: Towards a comprehensive look at global drivers of novel extreme wildfire events,
541 *Climatic Change*, 165, 43, 10.1007/s10584-021-03066-4, 2021.
- 542 Fire project — Climate Change Initiative: <https://climate.esa.int/en/projects/fire/>, last access: 9 October 2025.
- 543 ESA Climate Change Initiative Open Data Portal: <https://catalogue.ceda.ac.uk/uuid/3628cb2fdb443588155e15dee8e5352/>,
544 last access: 9 October 2025.
- 545 XFires: https://climate.esa.int/en/Cross_ECV_Projects/xfires/, last access: 24 March 2026.
- 546 Franquesa, M., Lizundia-Loiola, J., Stehman, S. V., and Chuvieco, E.: Using long temporal reference units to assess the spatial
547 accuracy of global satellite-derived burned area products, *Remote Sensing of Environment*, 269, 112823,
548 10.1016/j.rse.2021.112823, 2022.



- 549 García, M., Pettinari, M. L., Chuvieco, E., Salas, J., Mouillot, F., Chen, W., and Aguado, I.: Characterizing global fire regimes
550 from satellite-derived products, *Forests*, 13, 699, 10.3390/f13050699, 2022.
- 551 Ghasemiazma, F., Tonini, M., Fiorucci, P., and Turco, M.: Megafires in Mediterranean Europe: the compound role of fire
552 weather and drought, *npj Natural Hazards*, 3, 33, 10.1038/s44304-026-00197-5, 2026.
- 553 Giglio, L., Schroeder, W., and Justice, C. O.: The collection 6 MODIS active fire detection algorithm and fire products, *Remote
554 sensing of environment*, 178, 31-41, 10.1016/j.rse.2016.02.054, 2016.
- 555 Giglio, L., Schroeder, W., Hall, J. V., and Justice, C. O.: MODIS collection 6 and collection 6.1 active fire product user's
556 guide, National Aeronautical and Space Administration—NASA: Washington, DC, USA, 64, 2021.
- 557 Gincheva, A., Pausas, J. G., Torres-Vázquez, M. Á., Bedia, J., Vicente-Serrano, S. M., Abatzoglou, J. T., Sánchez-Espigares,
558 J. A., Chuvieco, E., Jerez, S., and Provenzale, A.: The interannual variability of global burned area is mostly explained by
559 climatic drivers, *Earth's Future*, 12, e2023EF004334, 10.1029/2023EF004334, 2024.
- 560 Guo, Z., Li, W., Ciais, P., Sitch, S., van der Werf, G. R., Bowring, S. P., Bastos, A., Mouillot, F., He, J., and Sun, M.:
561 Reconstructed global monthly burned area maps from 1901 to 2020, *Earth System Science Data Discussions*, 2025, 1-28,
562 10.5194/essd-17-3599-2025, 2025.
- 563 Hantson, S., Arneth, A., Harrison, S. P., Kelley, D. I., Prentice, I. C., Rabin, S. S., Archibald, S., Mouillot, F., Arnold, S. R.,
564 and Artaxo, P.: The status and challenge of global fire modelling, *Biogeosciences*, 13, 3359-3375, 10.5194/bg-13-3359-2016,
565 2016.
- 566 Hantson, S., Kelley, D. I., Arneth, A., Harrison, S. P., Archibald, S., Bachelet, D., Forrest, M., Hickler, T., Lasslop, G., and
567 Li, F.: Quantitative assessment of fire and vegetation properties in historical simulations with fire-enabled vegetation models
568 from the Fire Model Intercomparison Project, *Geoscientific Model Development Discussions*, 2020, 1-25, 10.5194/gmd-13-
569 3299-2020, 2020.
- 570 Jones, M. W., Abatzoglou, J. T., Veraverbeke, S., Andela, N., Lasslop, G., Forkel, M., Smith, A. J., Burton, C., Betts, R. A.,
571 and van der Werf, G. R.: Global and regional trends and drivers of fire under climate change, *Reviews of Geophysics*, 60,
572 e2020RG000726, 10.1029/2020RG000726, 2022.
- 573 Jones, M. W., Kelley, D. I., Burton, C. A., Di Giuseppe, F., Barbosa, M. L. F., Brambleby, E., Hartley, A. J., Lombardi, A.,
574 Mataveli, G., and McNorton, J. R.: State of wildfires 2023–2024, *Earth System Science Data*, 16, 3601-3685, 10.5194/essd-
575 16-3601-2024, 2024.
- 576 Kelley, D. I., Burton, C., Di Giuseppe, F., Jones, M. W., Barbosa, M. L., Brambleby, E., McNorton, J. R., Liu, Z., Bradley, A.
577 S., and Blackford, K.: State of Wildfires 2024–2025, *Earth System Science Data*, 17, 5377-5488, 10.5194/essd-17-5377-2025,
578 2025.
- 579 Laurent, P., Mouillot, F., Yue, C., Ciais, P., Moreno, M. V., and Nogueira, J. M.: FRY, a global database of fire patch functional
580 traits derived from space-borne burned area products, *Scientific Data*, 5, 1-12, 10.1038/sdata.2018.132, 2018.
- 581 Li, F., Zhang, X., Kondragunta, S., and Csiszar, I.: Comparison of fire radiative power estimates from VIIRS and MODIS
582 observations, *Journal of Geophysical Research: Atmospheres*, 123, 4545-4563, 10.1029/2017JD027823, 2018.



- 583 Linley, G. D., Jolly, C. J., Doherty, T. S., Geary, W. L., Armenteras, D., Belcher, C. M., Bliege Bird, R., Duane, A., Fletcher,
584 M. S., and Giorgis, M. A.: What do you mean, ‘megafire’?, *Global Ecology and Biogeography*, 31, 1906-1922,
585 10.1111/geb.13499, 2022.
- 586 Linley, G. D., Jolly, C. J., Doherty, T. S., Geary, W. L., Armenteras, D., Belcher, C. M., Bliege Bird, R., Duane, A., Fletcher,
587 M. S., and Giorgis, M. A.: ‘Megafire’—You May Not Like It, But You Cannot Avoid It, *Global Ecology and Biogeography*,
588 34, e70032, 10.1111/geb.70032, 2025.
- 589 Lizundia-Loiola, J., Franquesa, M., Khairoun, A., and Chuvieco, E.: Global burned area mapping from Sentinel-3 Synergy
590 and VIIRS active fires, *Remote Sensing of Environment*, 282, 113298, 10.1016/j.rse.2022.113298, 2022.
- 591 Lizundia-Loiola, J., Otón, G., Ramo, R., and Chuvieco, E.: A spatio-temporal active-fire clustering approach for global burned
592 area mapping at 250 m from MODIS data, *Remote Sensing of Environment*, 236, 111493, 10.1016/j.rse.2019.111493, 2020.
- 593 McFarland, J. R., Coop, J. D., Balik, J. A., Rodman, K. C., Parks, S. A., and Stevens-Rumann, C. S.: Extreme fire spread
594 events burn more severely and homogenize postfire landscapes in the southwestern United States, *Global Change Biology*, 31,
595 e70106, 10.1111/gcb.70106, 2025.
- 596 McKee, T. B., Doesken, N. J., and Kleist, J.: The relationship of drought frequency and duration to time scales, *Proceedings*
597 *of the 8th Conference on Applied Climatology*, Anaheim, California, 179-183,
- 598 Meyn, A., White, P. S., Buhk, C., and Jentsch, A.: Environmental drivers of large, infrequent wildfires: the emerging
599 conceptual model, *Progress in Physical Geography*, 31, 287-312, 10.1177/0309133307079365, 2007.
- 600 Mouillot, F., Schultz, M. G., Yue, C., Cadule, P., Tansey, K., Ciais, P., and Chuvieco, E.: Ten years of global burned area
601 products from spaceborne remote sensing—A review: Analysis of user needs and recommendations for future developments,
602 *International Journal of Applied Earth Observation and Geoinformation*, 26, 64-79, 10.1016/j.jag.2013.05.014, 2014.
- 603 Peters, A. J., Walter-Shea, E. A., Ji, L., Vina, A., Hayes, M., and Svoboda, M. D.: Drought monitoring with NDVI-based
604 standardized vegetation index, *Photogrammetric engineering and remote sensing*, 68, 71-75, 2002.
- 605 Peterson, D. A., Fromm, M. D., McRae, R. H., Campbell, J. R., Hyer, E. J., Taha, G., Camacho, C. P., Kablick III, G. P.,
606 Schmidt, C. C., and DeLand, M. T.: Australia’s Black Summer pyrocumulonimbus super outbreak reveals potential for
607 increasingly extreme stratospheric smoke events, *NPJ climate and atmospheric science*, 4, 38, 10.1038/s41612-021-00192-9,
608 2021.
- 609 Pinto, P., Silva, Á. P., Viegas, D. X., Almeida, M., Raposo, J., and Ribeiro, L. M.: Influence of convectively driven flows in
610 the course of a large fire in Portugal: the case of Pedrógão Grande, *Atmosphere*, 13, 414, 10.3390/atmos13030414, 2022.
- 611 Solano-Romero, E. and Segura-Garcia, C.: Extreme Fire Events EFEs database (Preliminar), Consorcio Madroño [dataset],
612 10.21950/TK9BXX, 2025.
- 613 Tedim, F., Leone, V., Amraoui, M., Bouillon, C., Coughlan, M. R., Delogu, G. M., Fernandes, P. M., Ferreira, C., McCaffrey,
614 S., and McGee, T. K.: Defining extreme wildfire events: Difficulties, challenges, and impacts, *Fire*, 1, 9, 10.3390/fire1010009,
615 2018.



- 616 Teymoor Seydi, S., Abatzoglou, J. T., Jones, M. W., Kolden, C. A., Filippelli, G., Hurteau, M. D., AghaKouchak, A., Luce,
617 C. H., Miao, C., and Sadegh, M.: Increasing global human exposure to wildland fires despite declining burned area, *Science*,
618 389, 826-829, 10.1126/science.adu6408, 2025.
- 619 University of Maryland: MCD14ML Active Fire Product (MODIS Collection 6) (Collection 6) [dataset], 2020.
- 620 Wilkinson, M. D., Dumontier, M., Aalbersberg, I. J., Appleton, G., Axton, M., Baak, A., Blomberg, N., Boiten, J.-W., da Silva
621 Santos, L. B., and Bourne, P. E.: The FAIR Guiding Principles for scientific data management and stewardship, *Scientific*
622 *data*, 3, 1-9, 10.1038/sdata.2016.18, 2016.
- 623 Williams, A. P., Hansen, W. D., Juang, C. S., Abatzoglou, J. T., Radeloff, V. C., Wang, B., Hall, J., Buch, J., and
624 Madakumbura, G. D.: The Western United States Large Forest-Fire Stochastic Simulator (WULFFSS) 1.0: a monthly gridded
625 forest-fire model using interpretable statistics, *Geoscientific Model Development*, 19, 1157-1191, 10.5194/egusphere-2025-
626 2934, 2026.
- 627 Yin, C., Abatzoglou, J. T., Jones, M. W., Cullen, A. C., Sadegh, M., Wang, J., and Liu, Y.: Increasing synchronicity of global
628 extreme fire weather, *Science Advances*, 12, eadx8813, 10.1126/sciadv.adx881, 2026.
- 629 Yool, S. R.: Enhancing fire scar anomalies in AVHRR NDVI time-series data, *Geocarto International*, 16, 7-14, 2001.
- 630